Nuclear Engineering and Technology 52 (2020) 1452–1461

Contents lists available at ScienceDirect

Nuclear Engineering and Technology

journal homepage: www.elsevier.com/locate/net

Original Article

Application and testing of a triple bubbler sensor in molten salts

A.N. Williams [a, *], A. Shigrekar [b], G.G. Galbreth [a], J. Sanders [a]

[a] Idaho National Laboratory, 2525 Fremont Ave, Idaho Falls, ID, 83402, USA
[b] University of Idaho, 1776 Science Center Dr., Idaho Falls, ID, 83402, USA

ARTICLE INFO

Article history:
Received 14 August 2019
Received in revised form
12 December 2019
Accepted 4 January 2020
Available online 7 January 2020

Keywords:
Bubble Pressure
Density
Vessel Level
Pyroprocessing
Process Monitoring
Nuclear Material Safeguards

ABSTRACT

A triple bubbler sensor was tested in LiCl–KCl molten salt from 450 to 525 °C in a transparent furnace to validate thermal-expansion corrections and provide additional molten salt data sets for calibration and validation of the sensor. In addition to these tests, a model was identified and further developed to accurately determine the density, surface tension, and depth from the measured bubble pressures. A unique feature of the model is that calibration constants can be estimated using independent depth measurements, which allow calibration and validation of the sensor in an electrorefiner where the salt density and surface tension are largely unknown. This model and approach were tested using the current and previous triple bubbler data sets, and results indicate that accuracies are as high as 0.03%, 4.6%, and 0.15% for density, surface tension, and depth, respectively.

1. Introduction

Electrochemical reprocessing (i.e., pyroprocessing) has been investigated worldwide as an alternative to traditional aqueous methods to recycle used nuclear fuel. In an application of this process, oxide fuels are declad and then reduced to a metallic form in an oxide reduction step. Following oxide reduction, the fuel is transferred into an electrorefiner (ER), and the useful uranium in the fuel is electrochemically dissolved and transported through a salt, where it deposits in purified form on a cathode [1]. During this electrorefining process, special nuclear materials (uranium and plutonium) accumulate in the salt. Using a liquid cadmium cathode (LCC) in the ER, uranium and plutonium can be co-extracted [2]. Thus, in a normally operating ER, the amounts of uranium and plutonium in the salt will constantly fluctuate, leading to nuclear material accountancy (NMA) and safeguards concerns. Using inductively coupled plasma mass spectrometry (ICP-MS) and/or other analytical techniques, information about the actinide concentration in the salt can be obtained. However, concentration data alone are not sufficient for material accountancy, because the salt volume is required to calculate the total mass of uranium, plutonium, and other actinides in the salt. The volume is best determined using the salt density, depth, and the volume of the vessel corresponding to the measured depth.

Means to measure the molten salt density and depth in the ER are extremely limited due to the high temperature, high radiation, inert gas environment, and remote operation of the electrorefining process (typically done in a hot cell). A frequently used approach to measure the salt depth is a cold dipstick method. In this approach, a cold metal rod is quickly inserted into the salt until contact with the vessel bottom is made and then it is quickly withdrawn. The height of salt adhering on the rod is then measured. Although this approach is suitable for process management, it lacks the accuracy and precision needed for material accountancy purposes. Kim et al. [3], at Korea Atomic Energy Research Institute (KAERI), developed a level sensor using a dynamic bubbler tube technique. With this approach, a tube with argon gas flow was lowered down into the molten salt. At the liquid-gas interface, a pressure spike is observed which can be used to determine the level in the vessel. Level measurements in a KNO_3 molten salt were determined to be within 1.1% at 500 °C.

Williams and co-workers [4,5] at Idaho National Laboratory (INL) developed and tested a triple bubbler sensor to determine the density, surface tension, and depth in aqueous solutions and molten salts. In this sensor, three bubbler dip-tubes (of Kovar metal) were fixed in an immersed position in the fluid. Tubes 1 and 2 were positioned at approximately the same depth in the fluid, but have different internal radii. The third tube is positioned

* Corresponding author.
E-mail address: ammon.williams@inl.gov (A.N. Williams).

https://doi.org/10.1016/j.net.2020.01.002

approximately 10 cm above the other two tubes and has approximately the same radius as Tube 1.

In the aqueous work [4], a model was developed using a derived governing equation for maximum bubble pressure which is as follows:

$$P = \rho g d + \frac{2}{3}\rho g r + \frac{2\gamma}{r} \quad (1)$$

where P is the measured pressure, ρ is the fluid density, g is the gravitational constant, d is the tube depth in the fluid, r is the tube inside radius, and γ is the fluid's surface tension. The first term on the right-hand side represents the hydrostatic pressure in the fluid at tube depth. The second and third terms are an expression of the excess bubble pressure (P_B) as derived by Parmelee and co-workers [6] and represent buoyancy and surface tension effects, respectively. In the developed model, equations for Tubes 1 and 3 were solved to obtain the fluid density (assuming the same tube radii). The formula for surface tension was acquired from Sugden [7]; it utilizes the pressures from Tubes 1 and 2. Finally, with expressions for density and surface tension, the depth was calculated directly using Equation (1) for Tube 1. To increase the accuracy for density and surface tension and to tailor the equations to the actual bubbler, empirical correction factors were applied to calibrate the system. This correction was not applied to the original governing equation but to the individual solutions for density and surface tension. This calibration was performed by splitting the experimental data set into calibration and validation sets. With the calibration, the triple bubbler was able to determine the density, surface tension, and depth to within 0.16%, 3.38%, and 0.31%, respectively in aqueous solutions.

Initial molten salt testing of the triple bubbler, performed at INL [5], was conducted in eutectic LiCl–KCl and eutectic CsCl–LiCl at different temperatures between 425 °C and 525 °C. Independent depth measurements of the salt were performed using a resistance contact sensor paired with a digital height gauge. In this study, the calibration model developed in the aqueous work was utilized with the LiCl–KCl measurements as the calibration set, and the CsCl–LiCl set as the validation. The percent differences between the independently determined density, surface tension, and depth and the calculated values were 0.4%, 18%, and 0.8%, respectively. Here, the accuracy of the sensor/model in predicting the density and depth was below the desired 1% mark for material accountancy. The accuracy of the surface tension measurement was quite poor.

The bubbler testing reported with the triple bubbler sensor demonstrated the accuracy of the sensor in aqueous and molten salt media. However, the calibration model developed requires accurate knowledge of fluid density and surface tension to make empirical corrections. Whereas using known salt properties are ideal for calibration and are often available for pure molten salts, it is difficult to accurately determine the salt properties in the ER following operation. This is because the electrolyte salt in the ER typically contains significant quantities of other elements and compounds. Additional shortcomings to the above studies were the limited number of data sets and experimental configurations that were available for validation and the method and material properties used to correct for thermal expansion of the tubes were not experimentally validated. Addressing the above shortcomings in previous triple bubbler experiments was the main goal. The approach to accomplishing these goals was to confirm the calculated thermal expansion visually in molten salt and perform bubbler testing in LiCl–KCl eutectic salt by generating additional validation and calibrations sets. Finally, excess pressure models from the literature were compared to previously reported triple bubbler data [4,5] to evaluate their performance and accuracy and to develop a modified calibration model to describe the triple bubbler system that does not require knowledge of the density and surface tension properties. The success of this work will significantly increase understanding of triple bubbler sensor technology in high temperature applications where limited calibration data are available.

2. Materials and methods

The triple bubbler sensor used in this current study was the same sensor used in the aqueous and preliminary molten salt experiments, and a full description of the sensor can be found in Williams et al. [4,5]. In summary, the sensor has a 316 stainless steel construction (handle and protective shroud) around the three main bubbler tubes (of Kovar metal) as shown in Fig. 1. A fourth tube (also in the sheath) was used to measure the atmospheric pressure above the salt. A Macor ceramic spacer was positioned between the handle and the furnace surface to electrically isolate the sensor from the ER, as well as to provide some thermal insulation. The bubbler tubes themselves were constructed from 6.35 mm outside diameter Kovar tubes that had been cold rolled at the tips to improve the tube circularity. Following rolling, a 45° chamfer was placed on the tips, and the inner radii of the tubes were reamed to 2.28, 1.27, and 2.29 mm for Tube 1, 2, and 3, respectively. The tubes were then welded to the 316 stainless steel handle and allowed to hang freely through the interior of the shroud. With this configuration, the tubes are fixed at the top and can expand and contract independently from the stainless steel shroud. The physical tubes' lengths at room temperature (from the Macor spacer down to the end of the rolled tip) were 54.29, 54.38, and 44.12 cm for Tubes 1, 2, and 3, respectively.

As part of the triple bubbler sensor system, an instrument panel containing flowmeters and pressure transducers was used to control, measure, and record data. The pressure data recorded were the differential pressure between the bubbler tube of interest and the atmospheric pressure (Tube 4). Three differential pressure transducers (two MKS Baratron 698A12 and one MKS Baratron 968A11) were used to monitor the bubbling pressures using MKS type 670 signal conditioners. Three digital mass flow controllers (GMA50 0-6 cm^3/min) were used to control the bubbler gas flow rate with an MKS 247D four-channel power supply. These components were integrated into a LABVIEW system in which pressure signals and flowrates were monitored and logged.

A transparent tube furnace (Thermocraft, Inc.) with a 30 cm heating zone was vertically positioned in a fume hood to allow the insertion of the triple bubbler (see Fig. 2). To support the bubbler and to provide a vessel for an inert atmosphere, a custom 53 cm tall × 6 cm diameter quartz crucible was manufactured. In addition, a custom quartz cap was made to slide into the retort tube which created a semi-seal (assisted with a silicone gasket). Within the quartz cap were ports for the bubbler, thermocouple, argon gas inlet, and argon gas outlet. The thermocouple was 6.35 mm diameter by 76.2 cm long and had 12 leads positioned at 50.8 mm increments. Two separate quartz crucibles were used in these experiments. In the first experiment, the crucible was 30 cm tall by 5.7 cm in diameter. The second crucible was 30 cm tall by 5.7 cm in diameter and had one flat face (4 cm wide) along the axis to reduce optical distortions (caused by the index of refraction of the fluid). Insertion of a 1 cm diameter rod 10 cm long was used as a means of displacing salt to change the salt depth in the crucible without changing the density or surface tension.

As part of the bubbler validation, independent measurements of the depth of the molten salt were needed. Depth measurements were not taken during the first experiment in the transparent furnace. In the second set, a conductivity probe approach was used

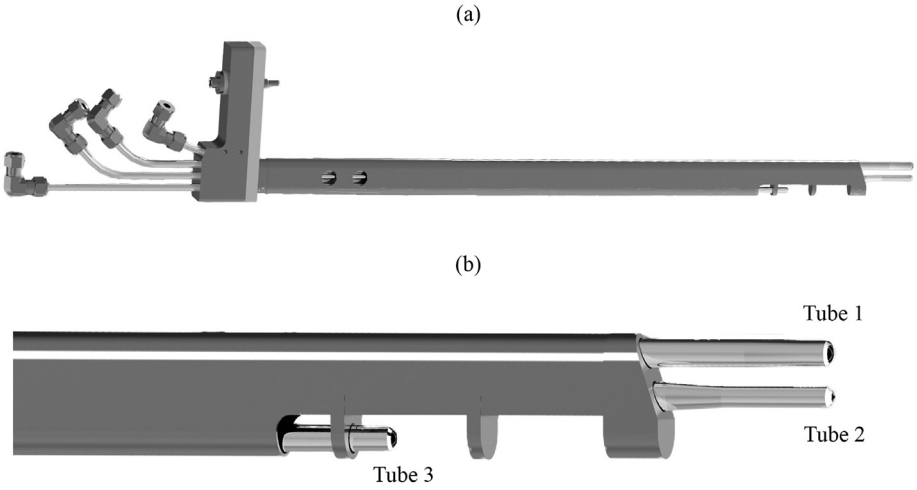

Fig. 1. 3D rendering of the triple bubbler sensor: (a) entire sensor and (b) close up of the three bubbler tube tips.

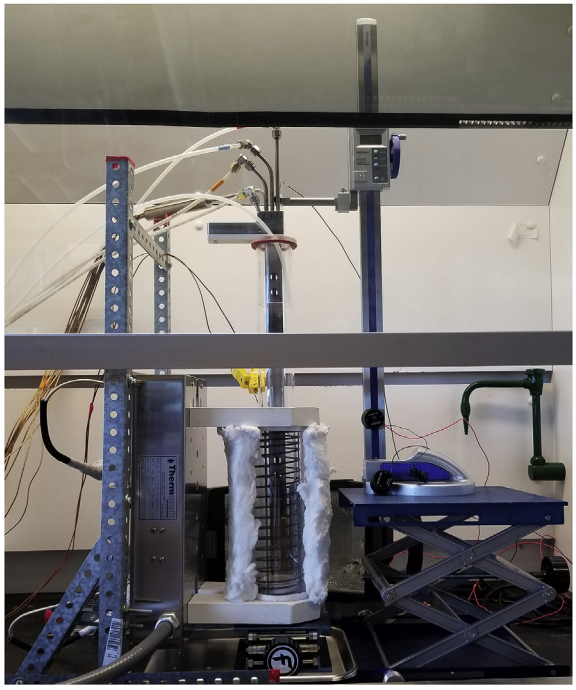

Fig. 2. Transparent furnace setup.

to measure the salt levels. In this approach, a wire wrapped quartz tube connected to a 600 mm digital height gauge (Mitutoyo 570-314), shown to the right in Fig. 2, was lowered into the 53 cm tall quartz crucible. The wire on the tube was connected to a light-emitting diode (LED) sensor, the other lead of which was connected to a thermocouple immersed in the salt. When the quartz rod (wire tip) came in contact with the top liquid surface, the circuit was completed and the LED illuminated. In this setup, the fume hood was not tall enough to allow for a measurement at the top of the quartz cap; consequently, the zero reference point used in these measurements was the bottom of the crucible, and the total depth of the salt was the only measurement achievable. This means that the 53 cm tall support crucible length, while at temperature, could not be measured directly.

Salts used in this study were LiCl–KCl eutectic (44 wt% LiCl). The bulk of the salt was from AAPL (anhydrous, 99.99% purity) and the other was mixed from LiCl (Alfa Aesar, 99.99%, ultra-dry) and KCl (Alfa Aesar, 99.99%, ultra-dry). In these tests, approximately 455 g of salt were used to achieve a salt depth of approximately 15–16 cm. The salt was weighed and added to the crucible in an inert atmosphere glovebox. The crucible was then covered with parafilm and transferred out of the glovebox and into the large quartz support crucible that had been backfilled with argon gas. With the salt in place, the quartz cap and argon gas lines were positioned. The bubbler and thermocouple were inserted into the crucible and hung just above the solid salt. Prior to heating, the retort tube was purged with argon gas at 10 L/min for 10 min. During heating and throughout the experiment, the gas flow rate was maintained at 5 L/min. The furnace was ramped up to the operating temperature at 4 °C/min. Once the salt was molten, the bubbler and thermocouple were lowered into the melt and allowed to come to steady state temperatures (~1 h). Photographs of the bubbler as well as pressure data were collected at four different steady-state temperatures; 450, 475, 500, and 525 °C.

Argon gas was bubbled through the molten salt, and the bubble pressures were recorded. At each temperature, a total of four to five replicate bubbler measurements were made. At the start of each replicate measurement, the temperature profile of the triple bubbler sensor and the salt level and depth were logged. In the case of the salt level and depth measurements, each set comprised of six replicate measurements. After these measurements were recorded, the bubbler control system recorded at least 10 min of pressure data. Following the pressure measurements, the depths and temperature profile were again recorded. This procedure provided before-and-after depth measurements and temperature profiles for every replicate pressure measurement set.

To measure the thermal expansion of the tubes at different temperatures, photographs of the bubbler tubes at various temperatures were taken using a digital camera (Canon D3200) positioned outside of the fume hood on a tripod. To reduce variation, each photo was scaled in the software ImageJ using the large tube (Tube 1) outside diameter. In addition, the crucible (low thermal expansion) had scribe-marks on both sides of the flat portion of the crucible at approximately 1 cm increments. A line was drawn between the two lowest marks (as shown in Fig. 3). This line was used as a reference from which tube growth was compared at different temperatures. The distance from the reference line to the bottom of the crucible was 11.5 ± 0.2 mm. Using ImageJ, the distance between the reference line and the bottom of the bubbler tubes were

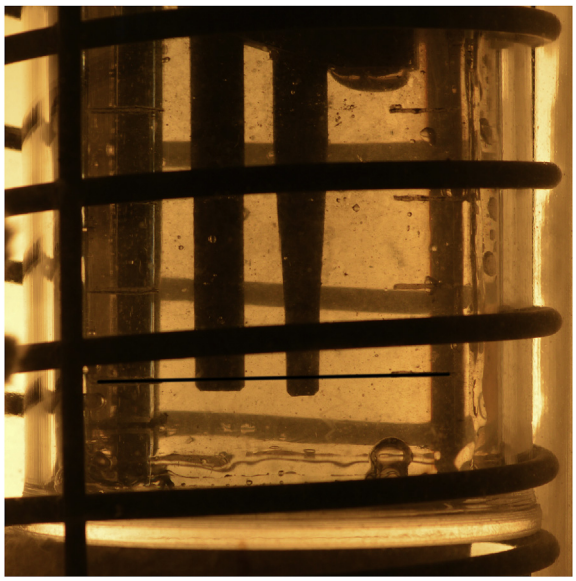

Fig. 3. Photo of the bubbler in LiCl–KCl salt at 450 °C. The reference line is shown in the photo.

recorded and then subtracted from the distance between the crucible bottom and reference line to arrive at the tube offset (j) from the bottom of the crucible.

3. Results

3.1. Thermal expansion

From the temperature profiles of the bubbler sensor in the salt, the thermal expansion could be calculated. The thermal expansion coefficients for Kovar metal as a function of temperature were reported by G. Galbreth [8]. The coefficients were $\alpha = -3.539 \cdot 10^{-9}$ T(°C)+$6.833 \cdot 10^{-6}$ up to 422 °C and $\alpha = 1.453 \cdot 10^{-8}$ T(°C)-$6.768 \cdot 10^{-6}$ up to 750 °C. Uncertainties on the coefficients were not reported and are were assigned to be ±10%. As the bubbler sensor operated under a continuous non-linear temperature profile, a MATLAB code was written to aid in the thermal expansion calculation. In this code, the length of the Kovar tubes was discretized into 1000 sections (approximately 0.56 mm long), each at an associated temperature, as determined from the measured temperature profile corresponding to that point. The change in length for each section was calculated, and the overall expansion was the sum of the individual sections. In order to relate the expected results with the photo analysis, the initial tube offset at room temperature was measured. To do this, the distance from the top of the quartz cap to the bottom of the crucible was measured using the height gauge, and then the cold bubbler-tube lengths were subtracted to arrive at the cold tube offsets which were 10.52 ± 0.04 and 9.91 ± 0.04 mm for j_1 and j_2, respectively. At the different temperatures, the tube offset could be estimated by subtracting the calculated thermal expansion (derived from the temperature profile) from the cold offset.

The first transparent furnace test was performed at several different temperatures using LiCl–KCl eutectic. However, the cylindrical crucible shape combined with the salt index of refraction acted as a lens and distorted the bubbler image (by compressing the image axially and stretching it radially). To reduce distortion effects, a second crucible was constructed with a flat face. For each temperature studied, 12 photographs were analyzed, and the tube lengths from the reference line were recorded. Table 1 shows the determinations of j_1 and j_2 from the photo analysis. The comparison between the photo-analysis approach and the temperature-based calculations is shown in Table 1. The photo-analysis approach and temperature-analysis estimations of the tube offsets were typically consistent (i.e., within uncertainty bands). However, in every case, the calculated thermal expansion was greater than the amount determined in the photo analysis. One explanation for this is that the quartz retort tube used in the experiments was assumed to be at constant length; in other words, it did not change with temperature. The expansion coefficient for quartz (10^{-7}) is one order of magnitude smaller than that of Kovar metal (10^{-6}). If the quartz were under the same temperature profile as the Kovar, the quartz thermal expansion would be approximately 0.12 mm over the 54 cm length. This change in length would shift (upwards) the bubbler-tube position with respect to the reference line, making the tube expansion appear less than it was. A correction was not made because the temperature profile of the quartz glass was unknown; however, this illustrates a potential bias in the photo-analysis approach. Despite the 3% difference between the two methods, the agreement between the two approaches is satisfactory, and the temperature-profile approach, with the reported coefficients, appears to be an accurate method for calculating thermal expansion (or the hot length) of the bubbler dip-tubes.

The uncertainties (function of the measured temperature and α) of the thermal expansion calculations were relatively low. As an example, at 500 °C, Tube 1 has a thermal expansion of 1.374 ± 0.004 mm. In determining the final hot length of the tube, the variances (s^2) of cold length and thermal expansion are added to arrive at the final tube uncertainty. In this case, the uncertainty is dominated by the cold-tube length.

3.2. Salt properties

The properties (density and surface tension) of the LiCl–KCl and CsCl–LiCl salts were not independently measured in this study. The values for these properties were determined from the literature. The density of LiCl–KCl eutectic was found in multiple sources [9–11] in which the determined values for the density at a given temperature were within 1.5% of each other. Data presented by G. Janz [10] has been most commonly used, so it was accepted as the true value in this study along with the originally reported uncertainties (0.01%). Two sources [9,10] were identified with surface tension correlations for LiCl–KCl salt. In this case, the difference between the surface tension values at a given temperature was approximately 5%. To be consistent with the density case, the correlation provide by G. Janz was selected in this study with uncertainties of ±0.87 mN/m or ~0.7%.

Although CsCl–LiCl was not used directly in this work, triple bubbler data previously collected using this salt will be analyzed; therefore, physical properties of the salt will be discussed here. Several literature findings for CsCl–LiCl were identified. Ito and Hasegawa [11] experimentally determined the density of CsCl–LiCl eutectic (59.3 mol% LiCl) salt below the temperature of 400 °C. No additional property correlations (density and surface tension) for eutectic CsCl–LiCl were found. However, G. Janz [10] had density and surface tension correlations for 55 mol% LiCl–CsCl and 70 mol% LiCl–CsCl within the temperature range between 577 °C and 761 °C. For both literature sources, the desired temperature range (425–525 °C) was outside of the reported range of the studies. An approximation of the density and surface tension was achieved by interpolating between the different mol% correlations to get values at 59.3 mol% LiCl. By extrapolation, the density and surface tension were determined in the temperature range of interest. For density, the difference between the interpolated Ito and Hasegawa [11] and the interpolated and extrapolated G. Janz [10] data was

Table 1
Comparison between the photographic analysis and the temperature-profile analysis.

	Photographic Analysis		Temperature Analysis			
°C	j_1 (mm)	j_2 (mm)	j_1 (mm)	j_2 (mm)	% diff (j_1)	% diff (j_2)
450	10.10 ± 0.23	9.34 ± 0.23	9.81 ± 0.09	9.20 ± 0.09	−2.95	−1.52
475	9.98 ± 0.23	9.26 ± 0.23	9.75 ± 0.10	9.14 ± 0.10	−2.30	−1.36
500	9.93 ± 0.23	9.21 ± 0.23	9.66 ± 0.10	9.05 ± 0.10	−2.72	−1.80
525	9.85 ± 0.23	9.11 ± 0.23	9.58 ± 0.11	8.97 ± 0.11	−2.78	−1.58

approximately 1.5%. Because data were available (via interpolation and extrapolation) for both density and surface tension from G. Janz [10], these correlations were accepted as the true values for this study. No comparison for CsCl–LiCl surface tension was available. Uncertainties on these interpolated and extrapolated uncertainties were estimated by multiplying the original uncertainty by a factor of three. This resulted in relative uncertainties of ~1.5%, which would make the Janz and Ito and Hasegawa density correlations consistent with each other.

3.3. Model development and calibration

As shown in Eq. (1), the measured bubbler pressure is a combination of the hydrostatic pressure and the excess bubble pressure. The hydrostatic pressure term is straightforward and will not be evaluated here. A number of different expressions have been developed to describe excess bubble pressure. For small capillaries the Young Laplace equation of the form

$$P_B = \frac{2\gamma}{r}, \tag{2}$$

where r is the tube inside radius and has been used to describe the excess bubble pressure [6,12,13]. Hosama et al. [14,15] developed a model to describe the bubble pressure using density, surface tension, and tube diameter in combination with shaping parameters. Finally, Parmelee and co-workers [6] developed an expression using surface tension and buoyancy effects, as shown in Eq. (1), for excess bubble pressure. The Parmelee et al. expression was the form used for all three bubbler tubes in the aqueous and preliminary molten salt experiments reported by INL [5]. However, in previous bubbler modeling, the system of equations was not solved directly; the expression for surface tension was taken from the literature.

A comparison between the excess bubble pressure models can be made by rearranging Eq. (1) such that the measured pressure minus the hydrostatic pressure is on the left-hand side of the equation, leaving the excess bubble pressure alone on the right-hand side, as shown in Eq. (3).

$$P - \rho g d = P_B \tag{3}$$

In the LiCl–KCl molten salt experiments previously reported by our team [5], pressure and depth were measured, and density and surface tension were known from the literature (everything on the left-hand side of Eq. (3) can be computed). On the right-hand side, the different models describing excess bubble pressure could be compared to other known data (from the left-hand side) to verify how well the model matches experimental data. Fig. 4(a – b) shows the values of the left-hand side (x-axis) vs the right-hand side (y-axis) for three different expressions or models of bubble pressure. For the comparison, only data collected during the LiCl–KCl experiment (reported in Williams et al.) are shown. The data points in Fig. 4(a) represents the two larger-diameter tubes, and the data in Fig. 4(b) is from the smaller-diameter tube. The root mean squared error (RMSE) between the data and the 1-to-1 line (for all three tubes combined) was 25.8, 15.8, and 12.7% for the Hosama, Young-Laplace, and Parmelee expressions, respectively. For larger-diameter tubes, the Parmelee and Hosama excess bubble pressure expressions have RMSE of 6.4 and 6.2%, respectively. For smaller-diameter tubes, the Young-Laplace excess bubble pressure expression has the lowest RMSE of 7.0%. The observation makes sense because the buoyancy term in Parmelee's expression comes into play as tube diameter increases. The smaller-diameter tube, though not a capillary, appears to be better modelled by the Young-Laplace excess bubble pressure expression. Thus, the best governing equations for the triple bubble appear to be tube specific. Using the Parmelee expression for Tubes 1 and 3 and the Young-Laplace expression for Tube 2 yields a total RMSE of 6.5%.

A combination of the Parmelee and Young-Laplace expressions had the lowest RMSE. However, there is still variation from unity in this system, and a calibration appears to be necessary to correct the governing equations. In the aqueous [4] and initial molten salt studies [5], a correction factor was applied directly to the solutions for density and surface tension, rather than to the governing equations. This correction factor approach worked to correct density and surface tension when they were known, but the expression for depth was not corrected.

It may be possible to add correction factors into the governing equations directly in the form of solvable constants. If the 2/3 and 2 constants in the excess pressure expressions (Parmelee and Young Laplace) were replaced with calibration constants, c_1 and c_2, respectively, it may be possible to correct the governing equations prior to solving for density, surface tension and depth. With these new constants, the following system of equations describing the total bubble pressures is as follows:

$$P_1 = \rho g d_1 + c_1 \rho g r_1 + \frac{c_2 \gamma}{r_1} \tag{4}$$

$$P_2 = \rho g (d_1 + dX_{12}) + \frac{c_2 \gamma}{r_2} \tag{5}$$

$$P_3 = \rho g (d_1 - dX_{13}) + c_1 \rho g r_3 + \frac{c_2 \gamma}{r_3} \tag{6}$$

where d_1 is the depth of Tube 1, dX_{12} is the differential distance between Tubes 1 and 2, and dX_{13} is the differential distance between Tubes 1 and 3. This system of equations has five unknowns: ρ, γ, d_1, c_1, and c_2. In a calibration fluid where density and surface tension are known (not the case in an ER), calibration constants can be solved for in a straightforward manner. Once the calibration constants are known, the three governing equations can then be solved directly to obtain expressions for density, surface tension, and depth. When the salt density and surface tension are not known (typical of an ER), it may be feasible to make an independent measurement of the salt depth using a resistivity contact sensor approach or, perhaps, a dynamic-bubbler approach, as outlined by Kim and coworkers [3]. If an independent depth (d_1) is available, a solution for c_1 can be obtained algebraically by first solving Eq. (4) for $c_2{}^*\gamma$ and then substituting that into Eqs. (5) and (6). This results

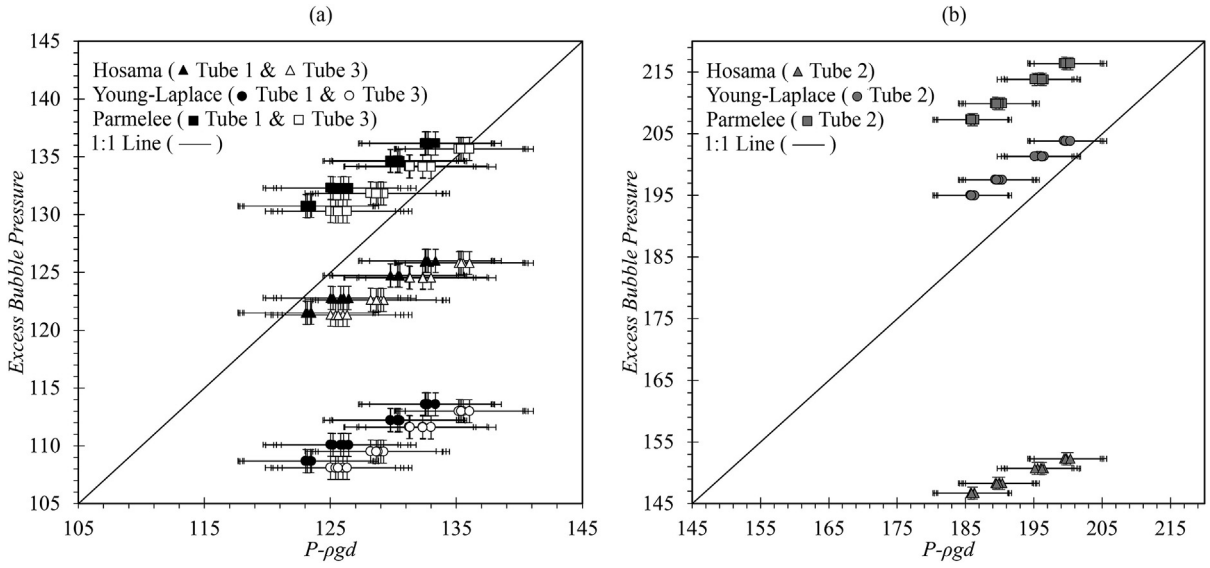

Fig. 4. Comparison between the excess bubble pressure (y-axis) from the various expressions and the measured pressure minus the hydrostatic pressure (x-axis). This data was generated in LiCl–KCl salt at 450, 475, 500, and 525 °C. (a) Data from Tubes 1 and 3 and (b) Data from Tube 2.

in a system of two equations, with ρ and c_1 as unknowns. The solution for c_1 is

$$c_1 = \frac{d_1[\varphi_2(r_3 - r_1) - \varphi_3(r_2 - r_1)] - \varphi_3 dX_{12} r_2 - \varphi_2 dX_{13} r_3}{r_1^2(\varphi_2 - \varphi_3) - \varphi_2 r_3^2} \quad (7)$$

where

$$\varphi_2 = P_2 r_2 - P_1 r_1 \quad \text{and } \varphi_3 = P_3 r_3 - P_1 r_1. \quad (8)$$

The above expression for the constant c_1 is a function of the depth and the measured pressures. Thus, with an independent depth measurement, it is possible to determine c_1 as a constant that satisfies the governing equations for the triple bubbler sensor. The constant c_2 cannot be separated from surface tension; thus, γ must be known to determine the value of c_2. As the surface tension of the salt in an ER is largely unknown, it is unlikely that the actual value of c_2 can be determined for that salt.

The new calibration approach was applied to the aqueous data reported by INL [4]. The aqueous data comprised eight different experiments using four different salt solutions (DI water, 21 wt% $CaCl_2$, 37 wt% $CaCl_2$, and 22.5 wt% NaCl). In each experiment, the fluid depth was increased incrementally (by adding solution) to provide three sets of measurements in the same fluid batch. Thus, a total of 24 data sets were acquired. For each data set, c_1 was calculated using Eqs. (7) and (8) with the independently measured depths. Following the calculation, the values were averaged to obtain a representative value for c_1. Errors were calculated as a combination of the data set standard deviation (in the averaging) as well as propagation of errors from r_1, r_2, r_3, P_1, P_2, P_3, dX_{12}, dX_{13}, and d_1. The averaging and error analysis resulting in a value for c_1 of 0.672 ± 0.063 (9.4% relative uncertainty). The depth contribution from the error analysis was only approximately 1%. The greatest contribution was from the pressure terms as the standard deviations in these data sets were high. The RMSE before and after the calibration were 2.85 and 2.89%, respectively, which are not significantly different from each other. Indeed, the calibration constant in this case is not statistically different from the original 2/3 value reported by Parmelee and co-workers [6].

The molten salt data from INL [5] were also used to determine the calibration constant using the new modelling approach. The independently measured depths (6 repetitions before and another 6 after each set) were averaged and, typically, had standard deviations of 0.05–0.08 mm. However, due to the small crucible diameter, it was not possible to make salt level measurements without some bias (systematic error) due to the salt meniscus. The best estimation is that approximately 0.1 mm of bias is present in the measurements, and the overall uncertainty of the depth measurements takes this systematic effect into account. An additional source of error for depth is from thermal expansion. Using the averaged depth and uncertainty from the calibration set yielded a c_1 value of 0.614 ± 0.05 (the standard deviation of the data was 0.016). In the propagation of errors analysis for c1, the depth uncertainty constituted approximately 30–40% of the total uncertainty. Unlike the aqueous calibration, the calibration constant is not quite consistent with the original 2/3 value (extremely close to being within the uncertainty bands). The calibration adjustment does reduce the RMSE down to 5.5% (from 6.5%).

Because the calibration constant in both the aqueous and molten salt cases are consistent (and nearly consistent with the original 2/3 value proposed), it may be possible that an additional calibration is not necessary with this new model approach. Going forward, both a calibrated and uncalibrated approach will be evaluated to explore the significance in the calibration.

The system of equations (Eqs. (4) – (6)) can be solved algebraically for density, depth, and surface tension, the solutions are as follows:

$$\rho = \frac{\lambda(P_1 - P_2) - \beta(P_1 - P_3)}{g(c_1\psi - \Omega)}, \quad (9)$$

where

$$\lambda = \frac{r_1 r_2}{r_2 - r_1},\ \beta = \frac{r_1 r_3}{r_3 - r_1},\ \psi = r_1(\lambda - \beta) + \beta r_3, \quad \text{and } \Omega = \beta dX_{13} - \lambda dX_{12} \quad (10)$$

$$d_1 = \frac{c_1(r_1^2(\varphi_2 - \varphi_3) - \varphi_2 r_3^2) + \varphi_3 dX_{12} r_2 + \varphi_2 dX_{13} r_3}{\varphi_2(r_3 - r_1) - \varphi_3(r_2 - r_1)} \quad (11)$$

$$\gamma = \frac{r_1 r_2}{c_2}\left[\frac{P_1(d_1 - dX_{12}) - P_2(d_1 + c_1 r_1)}{r_2(d_1 - dX_{12}) - r_1(d_1 + c_1 r_1)}\right] \quad (12)$$

As can be seen in Eqs. (9) – (12), the constant c_2 only appears in the surface tension formula, and the density and depth solutions are independent of the surface tension. Consequently, the assumption that c_2 is equal to 2 does not influence the calibration for density or depth. This assumption does, however, influence the accuracy of the surface tension measurement. For nuclear material accountancy purposes, only the depth and density are needed, so this calibration approach with an assumed c_2 correction is sufficient. However, if the surface tension of the fluid is available or can be measured independently, the ideal value of c_2 could be determined for the proposed model.

A way to explore how well the modelling results compare is to look at differences in how many standard deviations (σ) the modelled values are away from the true values. Fig. 5(a–c) shows the differences without using a calibration for the aqueous data sets. For density, the variation in the data points averages around 2.15 σ, suggesting that there is a bias where the modelled results are consistently smaller than the true value. Indeed, the modelled results are on average 0.23% smaller than the true values. For surface tension and depth, the average σ are −0.53 (1.4% larger) and −0.1 (0.02% larger), respectively. Generally, the results were all within 2 σ, with only two points laying outside of 3 σ. Fig. 5(d–f) shows the comparison with the calibration. The results for density are the same, meaning that the effect of correcting c_1 has a negligible effect on density. For surface tension and depth, the minor biases shifted to −0.42 (1.68% larger) and −0.001 (0.0001%), respectively. An additional change from the calibration was an increase in uncertainty; thus, the differences between the model and true values have less variation in terms of σ. Overall, applying the calibration did improve the results for depth, though the uncalibrated results were more than sufficiently accurate. As a result, a calibration does not seem necessary based on the aqueous data (though an additional correction to address the bias in density would be beneficial). For the aqueous data, the calculated density had a percent difference between 0.18 and 0.36%. For surface tension, the percent difference was between −4.9 and + 2.8%. Finally, for depth the percent difference was between −0.14% and +0.32%. The accuracies reported [4] for this data using the previous modeling approach were 0.16, 3.38, and 0.31% for density, surface tension, and depth, respectively.

The model, with and without calibration, was also applied to the LiCl–KCl molten salt data from Williams et al. [5]. Fig. 6(a–c) shows differences without applying the calibration. The average σ′s for density, surface tension, and depth were 2.27 (0.21% smaller), −0.58 (1.11% larger), and 1.42 (0.18% smaller), respectively. After applying the calibration as shown in Fig. 6(d–f), results for density were the same, which was consistent with the aqueous example. However, for surface tension and depth, the new average σ′s were 0.37 (1.04% smaller) and −0.01 (0.002% larger), respectively. Though the average σ for depth is close to zero, there is a noticeable linear upward trend in σ. This linear trend appears to be a function of the salt temperature. Potential explanations for this trend regarding the temperature are changes in the salt meniscus height that created biases not captured in this study, thermal expansion changes have not been fully addressed, and small changes are evidenced in the constant c_1 with temperature. The last is difficult to determine because it is a function of the measured depth, which the first two options influence. For molten salt data, the calibration does appear to be significant, because it did correct most of the bias for the depth and improved the bias in surface tension. The remaining bias present in the surface tension may be addressed if c_2 were included in the calibration.

In both the aqueous and molten salt cases, adjusting c_1 had little effect on the density, and the modelled values were 0.21–0.23% smaller than the true values. With closer evaluation of the results, the distribution of the data appears randomly centered around a constant bias; therefore, a correction factor may be applied to the density expression to improve accuracy. As the density does not appear in the expressions for surface tension or depth, this constant will only affect density. A correction factor of 1.0022 was selected; it will increase the modelled value by 0.22% (average between the two studies). With this correction, the average σ for the aqueous and molten salt densities were 0.17 and −0.17, respectively with the distribution of data being within 1 σ. Validation of this correction factor will be shown hereafter. However, without this correction,

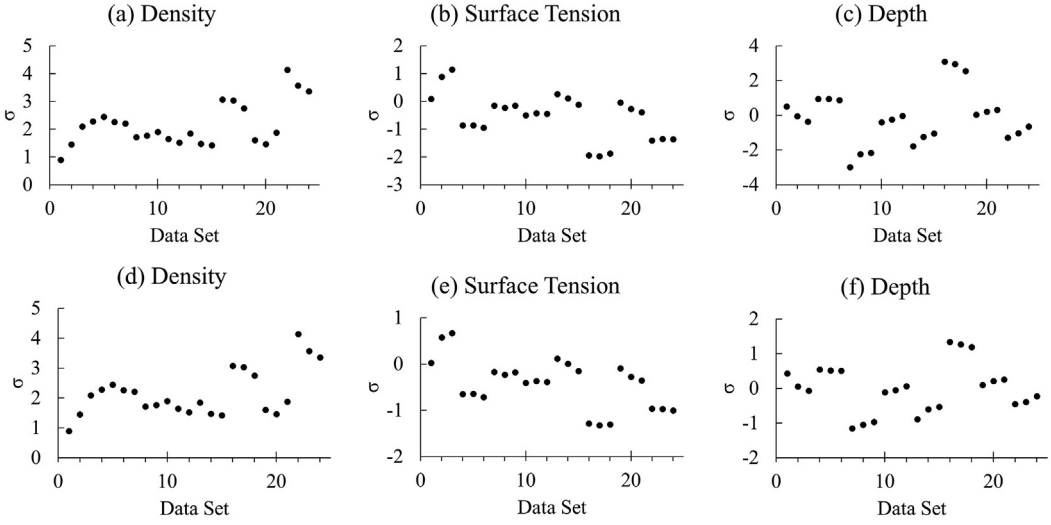

Fig. 5. Difference (number of standard deviations, σ) between the modelling results and the expected true values: (a–c) without calibration and (d–f) with c_1 calibration. The bubbler data was generated at ~20-24 °C in deionized water (data set #1-6), 21 wt% $CaCl_2$ solution (data set #7-12), 37 wt% $CaCl_2$ solution (data set #13-18), and 22.5 wt% NaCl solution (data set #19-24).

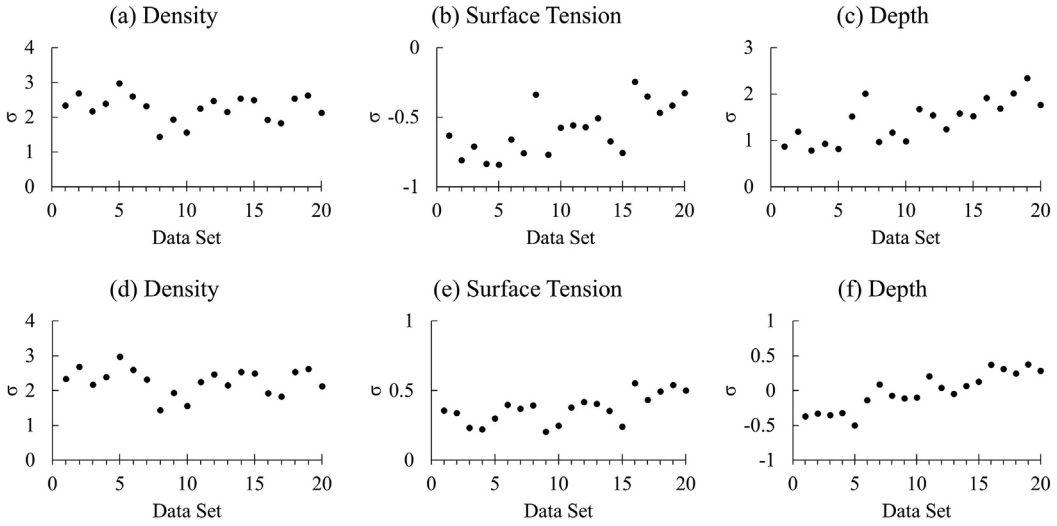

Fig. 6. Difference (number of standard deviations, σ) between the LiCl–KCl molten salt modelling results and the expected true values: (a–c) without calibration and (d–f) with c_1 calibration. The data shown was generated at four different temperatures: 450 °C (data set #1-5), 475 °C (data set #6-10), 500 °C (data set #11-15), and 525 °C (data set #16-20).

the uncertainty of the density measurement may be expanded by ~0.22% to address the bias.

3.4. Model validation

For the CsCl–LiCl molten salt data [5], the previously reported accuracies were 0.4%, 18%, and 0.8% for the density, surface tension, and depth, respectively. Appling the new modelling approach to the validation set yielded percent differences less than 0.03, 4.7, and 0.15% for density, surface tension, and depth, respectively. The relative error in these calculations was on average 0.17, 9.6, and 0.46% for density, surface tension, and depth. The distribution of values were within one σ.

3.4.1. Transparent furnace data

Data from the two transparent molten salt experiments conducted in this work were also used to validate modeling. The measured pressure profiles were somewhat sinusoidal as bubbles formed and broke at the bubbler tips. The maximum bubble pressure was determined using the "findpeaks" function in MATLAB for each bubble in the acquisition sequence. A common problem during these experiments was bubble interference from Tube 2. As the bubble on Tube 2 broke off, it created a disturbance in the surrounding fluid, which occasionally broke off the bubble on Tube 1 before the maximum pressure was reached. In addition, the bubble from Tube 2 would occasionally float up and knock off the bubble prematurely from Tube 3. The above interferences were reduced by adjusting the bubbler gas flowrate; however, the flow varied slightly over time, and some interference remained. As a result of these bubble interferences, outliers in the maximum bubbler pressure existed over the 10-min acquisition period. Because the extremes in the maximum bubble pressure are largely the result of bubble interferences, a boxplot method (a built-in MATLAB function) was used to identify and remove outliers from the data set. Following this step, the average and standard deviation of the maximum pressures were determined per acquisition period.

In the first experiment, depths were not measured, so only the density and surface tension properties can be compared. For density, the average σ was −0.28 with all of the measured values falling within one σ of the true values. The small bias of −0.28 σ represents only a difference of 0.05% between the measured and true values. For surface tension, all the modelled values fell within one σ of the true value, with an average sigma of 1.05. The bias of 1.05 σ represents a 4.6% difference between the modelled and true values. The relative uncertainties on the calculated values were 0.19, 4.64, and 0.29% for density, surface tension, and depth, respectively.

In the second transparent furnace experiment, the calculated density was within 2 σ of the true values, with an average σ of −1.44. This represented a difference of only 0.28% between the measured and true values (the calculated value is larger). For surface tension and depth, the calculated values were within one σ, with averages of 0.73 (5% difference) and 0.62 (0.21% difference), respectively. The relative uncertainty on the calculated values were 0.20, 7.04, and 0.35% for density, surface tension, and depth, respectively.

Table 2 shows the mean results with uncertainties from both the calibration sets and validation sets. Evaluating the density correction factor chosen via the three validation sets shows that the 1.0022 value tended to slightly overcorrect, more so with the transparent furnace experiments. Despite the slight overcorrection, the calculated values were within 1 σ, except in the case of the second transparent furnace experiment, for which the value was within 2 σ. The surface tension in the validation sets was typically within 1 σ, which shows good agreement between the calculated and true values. If c_2 were also included in the calibration, it is expected that the surface tension results would improve. The calculated depths in the validation set matched very well with the true value and were all within one σ. This result suggests that the selection of $c_1 = 0.614 \pm 0.05$ as a correction factor is indeed appropriate in the triple bubbler model in molten salts.

To further provide validation, for the second transparent furnace experiment, the depths were varied without affecting the density and surface tension using a quartz rod. As the quartz rod was lowered into the salt, it typically raised the salt level about 6.6 mm. This procedure did shift the temperature of the salt slightly, as shown in the table, but overall, the density and surface tension calculations were similar. The calculated depths shifted, as would be expected. This is important because many operations in the ER, such as adding and removing the anode/cathode, will displace salt and change the apparent depth of the salt. This test demonstrated that reasonable shifts in the salt level do not greatly influence the model or sensor accuracy. Changes in the density and surface tension were simulated via temperature changes.

Ideally, a calibration and validation approach would involve up

Table 2
Comparisons between the literature and calculated density, surface tension, and depth. The table shows data from the LiCl–KCl and CsCl–LiCl experiments [5] and the LiCl–KCl salt experiments generated in this work. In addition, the operating temperature for each data set is included in the first column of the table.

T (°C)	Literature (kg/m^3)		Bubbler (kg/m^3)		Literature (mN/m)		Bubbler (mN/m)		Contact Sensor (mm)		Bubbler (mm)	
	ρ	δρ	ρ	δρ	γ	δγ	γ	δγ	d	δd	d	δd
LiCl–KCl Molten Salt (Williams et al. [5], Calibration Set)												
456.4	1644.29	0.16	1644.58	1.34	129.5	0.9	128.5	3.5	148.56	0.14	148.67	0.31
475.7	1634.15	0.16	1634.82	1.57	127.9	0.9	126.7	3.7	149.26	0.15	149.29	0.33
505.2	1618.61	0.16	1618.31	1.62	125.5	0.9	124.2	3.5	150.34	0.15	150.31	0.32
524.7	1608.35	0.16	1608.62	1.50	123.9	0.9	122.1	3.6	151.42	0.14	151.32	0.32
CsCl-LiCl Molten Salt (Williams et al. [5], Validation Set)												
422.5	2423.01	1.10	2423.87	3.86	112.4	1.3	120.5	10.6	149.06	0.40	149.28	0.67
456.6	2394.73	0.93	2395.63	4.59	109.8	1.1	113.1	11.2	151.57	0.40	151.55	0.70
476.8	2377.95	0.82	2378.81	4.62	108.2	1.0	112.8	11.3	152.45	0.42	151.97	0.73
498.7	2359.80	0.71	2360.58	3.84	106.5	1.0	111.0	10.3	152.94	0.40	152.59	0.68
523.6	2339.21	0.59	2339.73	4.06	104.6	0.9	111.4	10.6	154.09	0.41	153.73	0.69
LiCl–KCl Molten Salt 1 (Transparent, Validation)												
400.4	1673.78	0.17	1675.42	2.37	134.1	0.9	128.4	4.9	–	–	150.43	0.40
449.5	1647.96	0.16	1648.14	3.86	130.1	0.9	126.4	6.6	–	–	153.03	0.45
475.8	1634.07	0.16	1635.07	3.02	127.9	0.9	121.8	5.5	–	–	154.53	0.44
497.3	1622.77	0.16	1623.91	3.43	126.1	0.9	118.7	5.9	–	–	156.03	0.49
526.0	1607.62	0.16	1607.54	2.97	123.8	0.9	117.3	5.6	–	–	157.41	0.47
LiCl–KCl Molten Salt 2 (Transparent, Validation)												
449.8	1647.77	0.16	1651.54	3.06	130.0	0.9	123.6	8.3	157.80	0.12	157.40	0.55
450.3	1647.53	0.16	1652.32	3.37	130.0	0.9	124.3	8.7	164.23	0.13	163.64	0.57
474.8	1634.61	0.16	1639.48	3.30	128.0	0.9	121.9	8.6	165.32	0.15	164.86	0.58
475.4	1634.30	0.16	1639.50	3.16	127.9	0.9	121.7	8.4	158.71	0.13	158.27	0.56
500.8	1620.91	0.16	1626.87	3.22	125.8	0.9	117.9	8.4	159.90	0.13	159.50	0.57
500.7	1620.95	0.16	1625.38	3.14	125.8	0.9	120.0	8.5	166.47	0.13	166.26	0.57
524.6	1608.39	0.16	1612.25	3.30	123.9	0.9	118.3	8.5	167.80	0.13	167.59	0.59
524.5	1608.42	0.16	1612.69	3.27	123.9	0.9	118.3	8.5	161.03	0.13	160.92	0.59

to five independent data sets, including several different salt compositions (to explore the composition effect). In this study, a total of four data sets were available. However, within those sets, the effect of temperature, depth, and salt composition (two salts) were evaluated. In addition, the selected salt compositions (LiCl–KCl and CsCl–LiCl) bracket the expected ER salt densities. Overall, the bubbler data fit well with independent measurements and literature correlations, giving confidence to the triple bubbler sensor and the modelling approach.

The new modeling approach and calibration method, as developed in this work, shows significant improvements in the accuracy over the initial model presented in Williams et al. [4,5]. In addition, this calibration approach can be implemented even when the fluid density and surface tension are not well known. Under conditions when the density and surface tension are unknown, and a direct comparison is not possible, the proposed model is anticipated to provide sufficiently accurate results (within 0.2%) for density and within 5% for the surface tension. The depth is part of the calibration approach and is therefore expected to perform proportionally to the quality of the independent depth measurements used in the calibration. In the current study, the independent depth measurements had absolute uncertainties of approximately 0.14 mm (for LiCl–KCl), which contributed approximately 30–40% to the uncertainty of c_1. The goal is to keep the uncertainties on the depth and density less than 1% for nuclear material accountancy. Estimating the minimum accuracy for an independent depth measurement is difficult because many factors contribute to the total uncertainty. However, in this study, if all other variables were kept the same, the minimum depth accuracy required to perform a calibration while maintaining the 1% total uncertainty goal is ±1.4 mm; this uncertainty would constitute ~98% of the uncertainty of c_1. In an actual hot cell environment containing an ER, it is anticipated that uncertainties of all variables will be greater, considering the nature of remote operations in a hot cell, narrowing the amount of uncertainty allowed on an independent depth measurement useful for calibration purposes. The 1.4 mm is provided simply as a rough upper range estimate of a value in which a calibration will certainly not yield sufficiently accurate results for nuclear material accountancy purposes. In cases in which independent depths cannot be measured with greater accuracy, a calibration is not recommended. However, the independent measurement, if consistent with sensor values, may provide some confidence to previous triple bubbler calibrations.

4. Conclusions

Several models were explored to determine the model that best matched the aqueous and molten-salt experimental data sets acquired previously. A simple combination of the Young-Laplace and Parmelee models yielded the best fit with a RMSE of 6.5% (in the molten salt case). However, a means to reduce this error were necessary to increase overall accuracy. The expression for the constant on the buoyancy term (c_1) was only a function of the depth and pressure of the fluid. Thus, c_1 could be determined from independent depth measurements in the calibration fluid, even when the fluid density and surface tension were unknown. The surface tension constant (c_2) can only be calculated when the surface tension of the fluid is known. However, the original model value of 2 was shown to provide accuracies of approximately 5% without a correction.

In the experimental data generated in this work (LiCl–KCl eutectic), the accuracies for density were between 0.05 and 0.28%. For surface tension the accuracies were 4.6 and 5%. Finally, for depth, the accuracy was 0.21%. In all three validation sets, the density and depth were well below the 1% mark desired for nuclear material accountancy purposes. As a result, the triple bubbler sensor and the proposed modelling approach shows great promise as an *in-situ* sensor for determining molten salt density and depth within an ER and other molten salt vessels used to processes used nuclear fuel.

Declaration of competing interest

The authors declare that they have no known competing financial interests or personal relationships that could have appeared to influence the work reported in this paper.

Acknowledgements

This work was supported by the U.S. Department of Energy (DOE) office of Nuclear Energy (NE), Nuclear Technology Research and Development (NTRD), Materials Protection, Accounting and Control Technologies (MPACT) campaign. Special thanks to Ron Wallace, Dean Burt, Guy Fredrickson, Brenda Serrano-Rodriguez, Michael Shaltry, DeeEarl Vaden, Tom Disanto, Carl Baily, and Tae-Sik Yoo for their assistance on this project. We also wish to thank the Center for Advanced Energy Studies (CAES) for laboratory support and space to conduct this research.

Appendix A. Supplementary data

Supplementary data to this article can be found online at https://doi.org/10.1016/j.net.2020.01.002.

References

[1] M.A. Williamson, J.L. Willit, Pyroprocessing flowsheets for recycling used nuclear fuel, Nucl. Eng. Technol. 43 (2011) 329–334.
[2] D. Vaden, S.X. Li, B.R. Westphal, K.B. Davies, T.A. Johnson, D.M. Pace, Engineering-scale liquid cadmium cathode experiments, Nucl. Technol. 162 (2008) 124–128.
[3] J. Kim, J. Lee, S. Bae, S. Paek, H. Kim, T. Kim, T. Park, Automated high-temperature liquid level measurement system using a dynamic tube pressure technique, J. Ind. Eng. Chem. 49 (2017) 30–35.
[4] A.N. Williams, G.G. Galbreth, J. Sanders, Accurate determination of density, surface tension, and vessel depth using a triple bubbler system, J. Ind. Eng. Chem. 63 (2018) 149–156.
[5] A.N. Williams, A. Shigrekar, G.G. Galbreth, J. Sanders, Application of a triple bubbler sensor for determining the density, surface tension, and depth in molten salts, J. Nucl. Mater. Manag. 47 (2019) 47–52.
[6] C.W. Parmelee, K.C. Lyon, C.G. Harman, The Surface Tensions of Molten Glass, vol. XXXVI, University of Illinois Bulletin, 1939, p. 8.
[7] S. Sugden, The determination of surface tension from the maximum pressure in bubbles. Part II, J. Chem. Soc. Trans. 125 (1924) 29.
[8] G.G. Galbreth, M. Shaltry, G.L. Fredrickson, D. Vaden, B.E. Serrano, Sensor for Measuring Density and Depth of Molten Salt, Idaho Natl. Lab., 2016. FY-16 FT-16INL04010404.
[9] M.V. Smirnov, V.P. Stepanov, Density and surface tension of molten alkali halides and their binary mixtures, Electrochim. Acta 27 (1982) 1551–1563.
[10] G.J. Janz, Thermodynamic and transport properties for molten salts: correlation equations for critically evaluated density, surface tension, electrical conductance, and viscosity data, J. Phys. Chem. Ref. Data 17 (1988).
[11] H. Ito, Y. Hasegawa, Densities of eutectic mixtures of molten alkali chlorides below 673K, J. Chem. Eng. Data 46 (2001) 1203–1205.
[12] K.J. Mysels, Improvements in the maximum-bubble pressure method of measuring surface tension, Langmuir 2 (1986) 428.
[13] K.J. Mysels, The maximum bubble pressure method of measuring surface tension, revisited, Colloids Surface. 43 (1990) 241–262.
[14] T. Hosama, M. Aritomi, T. Kawa, Numerical calculation and measurement of bubble shape and excess pressure in dip-tube pressure measurement, Nucl. Technol. 120 (1997) 121–135.
[15] T. Hosama, M. Aritomi, T. Kawa, Formulas to correct excess pressure and pressure shift to be used in volume measurement for plutonium nitrate solution, Nucl. Technol. 129 (2000) 218–235.